

Research Paper

Isogeometric Resolution of the Brinkman-Forchheimer-Darcy

Ouadie Koubaiti¹, Lahcen El Ouadefli², Ahmed Elkhalfi², Abdeslam El Akkad^{2,3}, Sorin Vlase⁴,
Marin Marin^{5,6}

¹ Department of Mathematics, MSISI, Laboratory, Faculty of Sciences and Techniques of Errachidia, Moulay Ismail University of Meknes, B.P. 509 Boutalamine, Errachidia, Morocco

² Mechanical Engineering Laboratory, Sidi Mohamed Ben Abdellah University, Faculty of Sciences and Techniques, B.P. 2202 Route Imouzzar, Fez, 30000, Morocco

³ Department of Mathematics Regional Centre for Professions of Education and Training (CREMF Fès-Meknès), Rue de Koweit 49, Ville Nouvelle, Fez, 30050, Morocco

⁴ Department of Mechanical Engineering, Faculty of Mechanical Engineering, Transylvania University of Brasov, Brasov, 500036, B-dul Eroilor 29, Romania

⁵ Department of Mathematics and Computer Science, Transylvania University of Brasov, Brasov, 500036, B-dul Eroilor 29, Romania

⁶ Academy of Romanian Scientists, Bucharest, 050045, Str. Ilfov, Nr. 3, Romania

Received December 01, 2023; Revised February 27, 2024; Accepted for publication March 20, 2024.

Corresponding author: M. Marin (m.marin@unitbv.ro)

© 2024 Published by Shahid Chamran University of Ahvaz

Abstract. In this paper, we employ the finite element method based on non-uniform rational B-splines function approximation to solve the nonlinear Brinkman-Forchheimer-Darcy equation in a simply connected and bounded Lipschitz domain Ω . We provide both theoretical and numerical studies of the Dirichlet boundary problem. Utilizing a stream function formulation, we demonstrate the well-posedness of the weak form. Furthermore, we approximate the velocity and pressure fields by linearizing the nonlinear terms, resulting in an algebraic system. This Non-uniform rational B-splines method is more effective in terms of the exact representation of the geometry and the good approximation of the solution compared to the virtual element method. To validate the effectiveness of the non-uniform rational B-splines Finite Element Method, we conduct numerical simulations of fluid flow in porous media.

Keywords: Brinkman-Forchheimer-Darcy, NURBS, FEM, Porous, Matlab, Stream formulation, Isogeometric analysis.

1. Introduction

A theoretical model for the flow of viscous, incompressible fluids in porous cavities is developed, focusing on the boundary problem associated with the Darcy-Forchheimer-Brinkmann system. This model is applicable to both bounded domains and simply connected boundary-connected domains.

The Darcy-Brinkman-Forchheimer (DBF) model emerges as a modification of the Stokes model, particularly suited for situations involving high permeability and porosity values. At high filtration rates, Darcy's law departs from linearity. Therefore, the DBF model incorporates the incompressible Navier-Stokes equations within a volume-averaged porous medium context, complemented by a closed model accounting for unknown terms in the volume-averaged equation. For comprehensive results, please refer to the following references [1-4]. This mathematical model demonstrates incompressible isothermal flow in porous media at steady state, in the case of fluid thermal coupling, this is the phenomenon of thermal non-equilibrium, one can see [5-7]. In the work [8], researchers examined cases where convective nonlinear terms are neglected, and the problem is unique to inhomogeneous Dirichlet boundary conditions. They have proven the existence of a solution for sufficiently infinitesimal source terms. Fabes et al. [9] have investigated the Dirichlet problem of the Stokes system in arbitrary Lipschitz domains in three dimensions ($n = 3$). They have established the well-posedness of the problem, guaranteeing the existence and uniqueness of weak solutions, provided the boundary data belong to the appropriate space. In [10], a stationary Navier-Stokes system with Dirichlet boundary conditions on a Lipschitz domain was constructed, considering data from the Sobolev space. Utilizing the Leray-Schauder theorem, existence of a solution was obtained, even when accounting for the Förcheimer term (as discussed in [11]). Uniqueness is preserved for terms with sufficiently small sources. When dealing with incompressible Navier-Stokes equations and homogeneous Dirichlet conditions, it is crucial to ensure a small data set for reliable problem-solving, as discussed in various references [12-15]. The equations governing velocity and pressure fields find applications in modeling fluid flow through porous media, which is essential for optimizing scenarios such as oil reservoirs [16]. While the Darcy equation serves as a reasonable model within a limited range of Reynolds numbers, it has limitations in accurately modeling flow in some densely packed porous media. In cases involving highly saturated, densely packed media with moderate flow velocities, characterized by very large Reynolds numbers, the flow becomes inherently nonlinear, surpassing the applicability of the linear Darcy equation.

The Brinkman equation is a special case of the (DBF) equation, it is very important in introducing a correction to Darcy's law to take into account viscous shear effects and changes in viscosity due to the introduction of a porous solid matrix. For more details



one can refer to [17, 18] which numerically solved this famous equation with the mixed finite element method and with the IGA method (Isogeometric Analysis).

A recently developed computational technique known as Isogeometric Analysis (IGA) seeks to bridge the gap between Computer-Aided Design (CAD) and Finite Element Analysis (FEA) [19-23], as introduced by Hughes et al. [24]. IGA operates on the isogeometric paradigm, employing the same basis functions used for representing known geometries to approximate unknown solutions to partial differential equations. IGA demonstrates its capacity to efficiently solve a wide range of numerical problems while ensuring accuracy.

A comprehensive discussion of the application of Isogeometric Analysis (IGA) to solve both linear and nonlinear equations for elastic and hydrodynamic problems can be found in [25].

IGA offers the optional use of globally smooth basis functions, enhancing its flexibility. In the standard Galerkin formulation for numerical approximation of higher-order Partial Differential Equations (PDEs), Non-Uniform Rational B-Splines (NURBS) provide distinct advantages. Their widespread utilization in Computer-Aided Design (CAD) technology, coupled with their mathematical properties, allows for global continuity of basis functions for $k > 0$ within the domain. This inherent advantage facilitates the solution of problems using a weak form of direct discretization, eliminating the need for mixed formulations like classical Finite Element Methods (FEM). In the realm of fluid dynamics, IGA has been employed to solve the Navier-Stokes-Korteweg isothermal equation, as detailed in the study of Gomez et al. [26], for modeling the isothermal gas-liquid phase transition. Other studies [27, 28] demonstrated the application of IGA in solving hull structure problems, specifically utilizing the Kirchhoff-Love model. Auricchio et al. [29] presented an application of IGA for solving a high-order equation, the stream function, in the context of addressing a plane elasticity problem. Additionally, it includes a numerical analysis of error convergence rates concerning point size, providing insights into the method's accuracy.

The novelty of this article lies in the application of a novel finite element method utilizing NURBS functions to address the Brinkman-Darcy-Forchheimer problem. We conduct a comprehensive examination of the validity of weak formulations, employing both stream functions and function space approximations for numerical solutions. Upon linearizing the nonlinear terms, our focus shifts to determining the components of the matrix involved in the algebraic problem at each iteration. Once we have assembled all the necessary matrices for this solution, we proceed to develop a complete Matlab code for solving the Navier-Stokes-Brinkmann problem, yielding significant numerical insights. The subsequent sections of this article will provide a detailed explanation of this process.

The paper is structured as follows: Section 2 introduces the governing equation. Section 3 discusses the weak formulation of the problem and establishes the existence and uniqueness of solutions using the stream function formulation. In Section 4, we provide an introduction to the basics of B-spline and NURBS functions, present the discrete problem, and discuss the linearization of the nonlinear term. Section 5 covers the presentation and discussion of numerical experiments conducted to validate our theoretical results. Finally, Section 7 draws conclusions and discusses future research directions.

2. The Governing Equation of Brinkman-Forchheimer-Darcy

We present a thorough investigation of the Dirichlet boundary problem for Darcy-Forchheimer-Brinkmann systems in bounded Lipschitz domains with connected boundaries. The system (1) and (2) calculates the velocity and pressure of an incompressible fluid in a porous medium.

Let $\Omega \rightarrow \mathbb{R}^n$, $n = 2,3$ represents porous medium and $\Gamma = \partial\Omega$ is its boundary,

$$-\operatorname{div}(\varepsilon\nu\nabla u - \varepsilon u \otimes u) + \frac{\varepsilon}{\rho}\nabla p + \sigma(u) = f \quad \text{in } \Omega, \quad (1)$$

$$-\operatorname{div}(\varepsilon u) = 0 \quad \text{in } \Omega, \quad (2)$$

The velocity and pressure are represented by $u: \Omega \rightarrow \mathbb{R}^n$ and $p: \Omega \rightarrow \mathbb{R}$, respectively.

The positive variable $\varepsilon = \varepsilon(x)$ represents the porosity, the fraction of the non-solid volume in the total volume of the material, and is generally spatially varying. f represents the external force (e.g., gravity), ρ is the constant density of the liquid, and ν is the constant kinematic viscosity of the liquid. The binomial product of u with itself is defined by the matrix notation $u \otimes u = (u_i u_j)_{ij}$. To model the impact of compression on inertial effects, the expression $\sigma(u)$ describes the frictional force caused by a packing of spherical particles of constant diameter, we use the equation given by Ergun [30]:

$$\sigma(u) = 150\nu \frac{(1-\varepsilon)^2}{\varepsilon^2 d_p^2} u + 1.75 \frac{1-\varepsilon}{\varepsilon d_p} |u|u. \quad (3)$$

where d_p represents the pellet diameter and $|\cdot|$ represents the Euclidean vector norm. The first order term in (1) accounts for the Darcy pressure drop and the second order term is Forchheimer's law. Models (1)-(2) with pressure terms of the form $\nabla(\varepsilon p)$ were proposed in section 2.2 of [31]. Also, see [32-37] and Chapter 1 of [38] for the derivation of the equation, its limitations, and modeling and homogenization issues in porous media. we prescribe Dirichlet boundary condition:

$$u|_{\Gamma} = g. \quad (4)$$

The following applies $\int_{\Gamma_i} \varepsilon g \cdot n ds = 0$, all connected components Γ_i of the boundary Γ must be satisfied. It is assumed that the porosity distribution ε satisfies the constraints:

$$0 < \varepsilon_0 \leq \varepsilon(x) \leq \varepsilon_1 \quad \forall x \in \Omega, \quad (5)$$

with some constants:

$$0 < \varepsilon_0, \varepsilon_1 \leq 1. \quad (6)$$

Depending on the Reynolds number outside the range of Darcy's law, fluid flow through a porous medium can be fully described. For further details see [39]. See also [40] for information on how to use such a nonlinear Darcy-Forchheimer law to simulate pump levels in mining wells, and [41, 42] for current references on this model.

In the following part, taking into account the channeling effect near the wall, we address the porosity distribution estimated for a bed filled with spherical particles. This type of porosity distribution follows assumption (5)-(6). we resize in the following way:



$$u^* = \frac{u}{U_0}, p^* = \frac{p}{\rho U_0^2}, \tag{7}$$

$$X^* = \frac{x}{d_p}, g^* = \frac{g}{U_0}, \tag{8}$$

where U_0 defines the size of the reference velocity. The asterisk is omitted for clarity. Then the Darcy-Brinkman-Forchheimer equation for the region $\Omega \subset \mathbb{R}^2$. Γ is the boundary and n is the outer normal vector. Then, we have:

$$-div\left(\frac{\varepsilon}{Re}\nabla u - \varepsilon u \otimes u\right) + \varepsilon \nabla p + \frac{\alpha}{Re}u + \beta u|u| = f \quad \text{in } \Omega, \tag{9}$$

$$div(\varepsilon u) = 0 \quad \text{in } \Omega, \tag{10}$$

$$u = g \quad \text{on } \Gamma. \tag{11}$$

where: $\alpha(x) = 150 k^2(x)$, $\beta(x) = 1.75 k(x)$, $k(x) = \frac{1-\varepsilon(x)}{\varepsilon(x)}$ and the Reynolds number is defined by $Re = \frac{U_0 d_p}{\gamma}$.

3. Weak Form in the Stream Function Formulation

The homogeneous Dirichlet boundary conditions for the velocity are defined in the case of $g = 0$. Then look for weak solutions to the Darcy-Brinkman-Forchheimer equation in the space:

$$X = H^1(\Omega)^n, \tag{12}$$

$$Q = \{q \in L^2(\Omega) : \int_{\Omega} q dx = 0\}, \tag{13}$$

let:

$$X_0 = [H_0^1(\Omega)]^n, M = L_0^2(\Omega) = Q, \tag{14}$$

$$V := X_0 \times M, \tag{15}$$

$$X_g = \{v \in X \setminus v = g\}, \tag{16}$$

Let us group the functions belonging to spaces X and X_g into spaces D and D_g , respectively, such that their divergence is zero:

$$D := \{v \in X \setminus div v = 0\}, \tag{17}$$

$$D_g := \{v \in X_g \setminus div v = 0\}. \tag{18}$$

Moreover, it is assumed that the Ω domain is connected (see [34-36]).

For all $v \in D$, there exists a unique $\vartheta \in H^2(\Omega)$ such as $v = \text{curl}(\vartheta)$, Curl is the partial differential operator for scalar fields, defined as follows:

$$\text{curl}(\vartheta) = \left(\frac{\partial \vartheta}{\partial y}, -\frac{\partial \vartheta}{\partial x}\right), \tag{19}$$

with $n = 2$ or 3 . Where additional conditions on Q are required to guarantee uniqueness of the pressure, then the pressure is indeterminate up to a constant. Derive the variational formulation by taking the dot product of the momentum equation with the test function $v \in V$ and the continuity equation with the test function $q \in Q$. Multiplication and integration by parts of the momentum and mass balance and the test function $v \in X_0$ or $q \in M$ in (6) implies a weak formulation. Applying Green's formula and homogeneous Dirichlet boundary condition,

For all $v \in V$:

$$-\int_{\Omega} div\left(\frac{\varepsilon \nabla u}{Re}\right) \cdot v dv + \int_{\Omega} div(\varepsilon u \otimes u) \cdot v dv + \int_{\Omega} \varepsilon \nabla p \cdot v dv + \int_{\Omega} \frac{\alpha}{Re} u \cdot v dv + \int_{\Omega} \beta u|u| \cdot v dv = \int_{\Omega} f \cdot v dv, \tag{20}$$

$$\int_{\Omega} div(\varepsilon u) q = 0, \quad \forall q \in Q, \tag{21}$$

Then from the remark 1 in [33], we have: $div(\varepsilon u \otimes u) = \varepsilon(u \cdot \nabla)u$, we obtain for all $v \in V$:

$$\int_{\Omega} \nabla\left(\frac{\varepsilon u}{Re}\right) : \nabla v dv + \int_{\Omega} \varepsilon(u \cdot \nabla)u \cdot v - \int_{\Omega} \nabla p \cdot v dv + \int_{\Omega} \frac{\alpha}{Re} u \cdot v dv + \int_{\Omega} \beta u|u| \cdot v dv = \int_{\Omega} f \cdot v dv, \tag{22}$$

$$\int_{\Omega} div(\varepsilon u) q = 0, \quad \forall q \in Q, \tag{23}$$

The trilinear, bilinear, linear, and semi-linear forms will now be presented:

$$\begin{aligned} a: & X \times X \rightarrow R \\ b: & X \times Q \rightarrow R, \\ c: & X \times X \rightarrow R, \end{aligned} \tag{24}$$



Furthermore, we also define the non-linear forms as follows:

$$\begin{aligned} d: X \times X \times X &\rightarrow R, \\ n: X \times X \times X &\rightarrow R, \end{aligned} \quad (25)$$

We installed:

$$\begin{aligned} A(u, v) &:= a(u, v) + c(u, v), \\ N(w, u, v) &:= n(w, u, v) + d(w; u, v), \end{aligned} \quad (26)$$

Find $(u, p) \in X_0 \times M$ with $u|_{\Gamma} = g$, such that:

$$A(u, v) + N(u, u, v) - b(v, p) = (f, v) \quad \forall v \in X_0, \quad (27)$$

$$b(u, q) = 0 \quad \forall q \in M, \quad (28)$$

according to the properties of the curl operator, there is an isomorphism between the spaces: D, D_g and $\phi = \{\vartheta \in H^2(\Omega) \setminus \text{curl}\vartheta = 0 \text{ on } \Gamma\}$, $\phi_g = \{\vartheta \in H^2(\Omega) \setminus \text{curl}\vartheta = g \text{ on } \Gamma\}$, respectively. We rewrite the problem (27) by using the stream function $v \in \phi_g$. We make a change of variable $u = \text{curl}\vartheta$ is a velocity field solution problem (27). This later becomes:

Find $\vartheta \in \phi$ such as:

$$A_{\text{curl}}(\vartheta, v) + N_{\text{curl}}(\vartheta, \vartheta, v) = L_{\text{curl}}(v), \quad \forall v \in \phi, \quad (29)$$

where:

$$A_{\text{curl}}(\vartheta, v) = \frac{1}{Re} (\varepsilon \nabla \text{curl}(\vartheta), \nabla \text{curl}(v)), \quad (30)$$

$$N_{\text{curl}}(w, \vartheta, v) = ((c \text{curl}(w) \cdot \nabla) \text{curl}(\vartheta), \text{curl}(v)) + (\beta |\text{curl}(w)| \text{curl}(\vartheta), \text{curl}(v)), \quad (31)$$

$$L_{\text{curl}}(v) = (f, \text{curl}(v)). \quad (32)$$

The problem (29) is called the stream function formulation of the nonlinear Brinkman-Forchheimer-Darcy equation. The pressure field in Eq. (27), can be found by solving a second-order partial differential equation according to the stream function [43, 45].

Lemma:

The bilinear form A_{curl} , the trilinear skew-symmetric form N_{curl} and the linear L_{curl} form are continuous, then we have:

$$|A_{\text{curl}}(\vartheta, v)| \leq \frac{1}{Re} |\vartheta|_{H^2(\Omega)} |v|_{H^2(\Omega)}, \quad \forall \vartheta \in \phi_g, \forall v \in \phi, \quad (33)$$

$$|N_{\text{curl}}(w, \vartheta, v)| \leq C_{N_{\text{curl}}} |w|_{H^2(\Omega)} |\vartheta|_{H^2(\Omega)} |v|_{H^2(\Omega)}, \quad \forall w, \vartheta \in \phi_g, \forall v \in \phi, \quad (34)$$

$$|L_{\text{curl}}(\vartheta)| \leq |\vartheta|_{H^2(\Omega)} |f|_{H^2(\Omega)}, \quad \forall \vartheta \in \phi_g. \quad (35)$$

For some positive constant $C_{N_{\text{curl}}} > 0$ dependent on physical constants ε and β .

The results of the lemma are justified in the references [30-32].

Theorem:

With the condition of the continuity in the previous lemma of the bilinear form, the trilinear form and the linear form: $A_{\text{curl}}, N_{\text{curl}}(w, \vartheta, v), L_{\text{curl}}$ respectively. Moreover the property of the coercivity of the bilinear form A_{curl} , and $f \in H^1(\Omega)$. If the the data satisfies the following smallness condition: $Re \leq (CC_{\text{shape}} C_{N_{\text{curl}}} \|f\|_{H^1(\Omega)})^{\frac{1}{2}}$, where:

$$C = \sup_{\theta \in H_0^1(\Omega)} \frac{\|\theta\|_{L^2(\Omega)}}{\|\theta\|_{H^1(\Omega)}^2}, \quad (36)$$

C_{shape} is a strictly positive constant has been defined in Theorem 3.1 in [35], then, there exists a unique solution $\vartheta \in \phi$ of problem (29). When the following stability estimate holds:

$$|\vartheta|_{H^2(\Omega)} \leq CC_{\text{shape}} Re \|f\|_{H^1(\Omega)}, \quad (37)$$

The previous results thus established and adapted to our Darcy-Brinkman-Forchheimer problem are results that were provided in [44-46].

We now recall the following results from [38] when extending the existence and uniqueness of the results of solutions in the literature on flow problems in porous media, based on Brinkman-Forchheimer's non-linear Darcy extension law. This result is only valid for constant porosity without taking into account convective effects, and the results are also valid for variable porosity, which includes convective effects (See Ref. [38]).

4. B-spline and NURBS Basis Functions

NURBS is the industry standard for Computer-Aided Design (CAD) systems. More recently, it has grown significantly in popularity among computational mechanics experts, largely because of the work of Hughes et al. [39]. They used NURBS in their research as shape functions within the finite element framework, which led to the creation of an advanced FEM called isogeometric analysis (IGA). Since then, IGA has found applications in a wide range of problem domains.



In the context of NURBS, consider defining a vector $a = (a_1, a_2, \dots, a_{n+p+1})$. The knot values, denoted as a_i , where i ranges from 1 to $n + p + 1$, represent non-decreasing numbers that serve as coordinates in the parametric space. An interval $[a_i, a_{n+p+1}]$ is referred to as a 'patch' and is composed of 'knot spans' $[a_i, a_{i+1}]$, $i \in [1, \dots, n + p + 1]$, where i varies from 1 to $n + p + 1$. Knot vectors can be classified as either 'uniform' or 'non-uniform,' depending on whether all knot values are equally spaced or not. An 'open' knot vector is one where the first and last knots are repeated $p + 1$ times. For clarity, a B-spline basis function of order 0 will be defined as:

$$B_i^0(x) = 1 \text{ if } a_i \leq x \leq a_{i+1}, \tag{38a}$$

$$B_i^0(x) = 0 \text{ otherwise,} \tag{38b}$$

and defined as follows for B-spline basis functions of order $p > 1$:

$$B_i^d(x) = \frac{x - a_i}{a_{i+d} - a_i} B_i^{d-1}(x) + \frac{a_{i+d+1} - x}{a_{i+d+1} - a_{i+1}} B_{i+1}^{d-1}(x), \quad d = 1, \dots, p. \tag{39}$$

A representation of a B-spline basis function is shown in Fig. 1. NURBS basis functions are rational B-spline functions. In order to define them, a collection of positive weights is used $\omega_i, i = 1, \dots, n$.

Let define the function:

$$R_i^p(x) = \frac{\omega_i B_i^p(x)}{\sum_{j=1}^n \omega_j B_j^p(x)},$$

that is, if the internal nodes are not repeated, NURBS basis functions are C^{p-1} -continuous. The basis of a node in a knot with multiplicity k is C^{p-k} -continuous. A linear combination of a NURBS basis function of order p and n control points P results in a NURBS curve of order p . The NURBS curve is described as:

$$C(x) = \sum_i^n R_i^p P_i(x), \tag{40}$$

that P_i the control points built the control polygon. The definition of bivariate NURBS in 2D is:

$$N_{i,j}^{p,q}(x,y) = \frac{B_i^p(x) B_j^q(y) \omega_{ij}}{\sum_k^n \sum_l^m B_k^p(x) B_l^q(y) \omega_{kl}}. \tag{41}$$

On the one side, we have the physical domain, and on the other side, we find the reference domain. In the reference domain, numerical techniques, such as the Gaussian method, are employed to approximate integrals. When moving from a weak formulation to a matrix formulation, this method is useful for optimizing the computation of matrix elements. The tensor product of B-spline basis functions allows NURBS curves to be extended to NURBS surfaces and volumes. This is how a NURBS surface is described:

$$S: [0,1]^2 \rightarrow \mathbb{R}^2 S(\xi_1, \xi_2), = (x_1(\xi_1, \xi_2), x_2(\xi_1, \xi_2)) S(\xi_1, \xi_2), \tag{42}$$

NURBS are parameterized based on two coordinates, (ξ_1, ξ_2) . A B-spline basis function is applied with polynomial orders p and q , and a control mesh is formed by n by m control points. The weights ω_{ij} corresponding to the definition of the NURBS basis do not follow the tensor product structure and, like the control points P_{ij} , can be chosen arbitrarily. NURBS volumes can also be formulated in a similar way.

The derivation of the NURBS parameterization in terms of parameter coordinates is straightforward and applicable supports any order of NURBS basis functions.

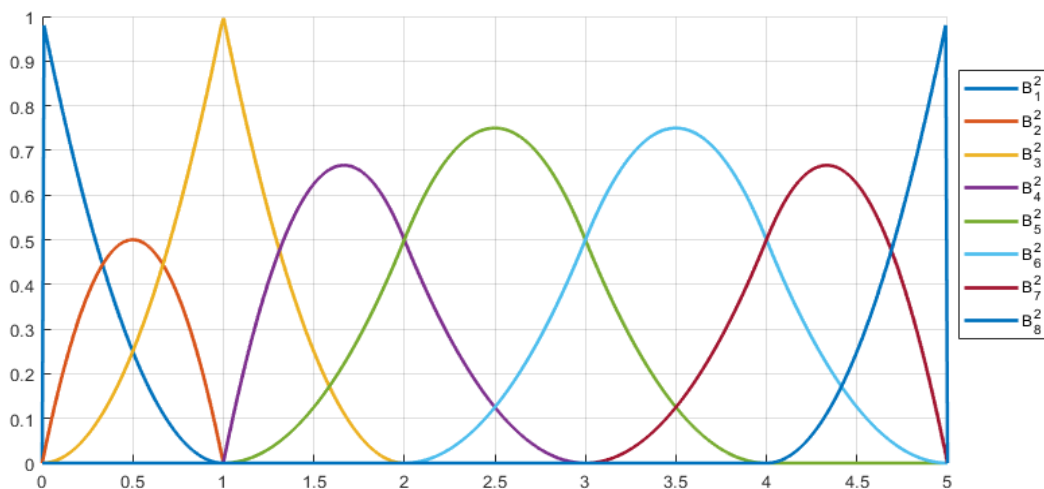


Fig. 1. B-spline basis functions defined by the node vector $\Xi = \{0,0,0,1,1,2,3,4,5,5,5\}$.



5. Approximation Problem

5.1. Iterative form

We take the same approach as [41] by deploying the extension $G \in X$ of g , which validates $\text{div}(\varepsilon G) = 0$. As a result, $w \in X_0$ has the value $u = w + G$. Inferring that w is the answer to the following problem. From the problem (27) to (28):

$$A(w, v) + N(w + G, w + G, v) - b(v, p) = (f, v) - A(G, v), \quad (43)$$

We consider the functional spaces $X_{0h} \subset X$ generated by second order NURBS functions as defined in (41), such that verify $u = 0$ on Γ and $M_h \subset M$ generated linear NURBS.

Before solving an algebraic problem, we must first linearize the nonlinear problem (43) and for this we introduce the following iterative algorithm:

Suppose initially guess $w_h^0 \in X_{0h}$ and at each iteration j , we compute the solution of the unknown pair (w_h^j, p_h^j) :

$$A(w_h^{j+1}, v_h) + N(w_h^j + G, w_h^{j+1}, v_h) - b(v_h, p_h^{j+1}) = (f, v_h) - A(G, v_h) - N(w_h^j + G, G, v_h), \quad (44)$$

At the j th iteration, we wish to discover approximate values for the velocity $u_h^j: [0,1]^2 \rightarrow \mathbb{R}$ and pressure $p_h^j: [0,1]^2 \rightarrow \mathbb{R}^1$, which are linear combinations of the previously stated basis functions.

Only geometry can be represented with NURBS. We will use them to roughly approximation the variables velocity u and pressure p in order to assess their performance:

$$u_{hk}^j(\xi_1, \xi_2) = (w_{hk}^j + G)(\xi_1, \xi_2) = \sum_i^n N_i^{p,q}(\xi_1, \xi_2) u_{ik}^j, \quad (45)$$

$k = 1, 2$ in (45) denotes the two components velocity field:

$$p_h^j(\xi_1, \xi_2) = \sum_i^m N_i^{r,s}(\xi_1, \xi_2) p_{hi}^j, \quad (46)$$

n and m are the number of basis functions of velocity and pressure, while u_{ik}^j and p_{hi}^j are unknown control variables for velocity and pressure at the j th iteration we want to determine. The velocity and pressure fields in equations (45)-(46) are defined in parameter space, with the main equations (1)-(2) given in physical space.

In order to evaluate fields in physical space, the pressure $p: \Omega \rightarrow \mathbb{R}^2$ on the physical domain and the velocity $u: \Omega \rightarrow \mathbb{R}^2$ on the physical domain are calculated using the inverse function S^{-1} of the geometric parameter S defined in (42). The geometry parametrization's Jacobian matrix is defined as J as follows:

$$J = \begin{bmatrix} \frac{\partial x_1}{\partial \xi_1} & \frac{\partial x_1}{\partial \xi_2} \\ \frac{\partial x_2}{\partial \xi_1} & \frac{\partial x_2}{\partial \xi_2} \end{bmatrix}, \quad (47)$$

the pressure gradient in the parameter space: $\widehat{\nabla} p = J \nabla p = \begin{pmatrix} \frac{\partial p}{\partial \xi_1} \\ \frac{\partial p}{\partial \xi_2} \end{pmatrix}$, with: $\nabla p = \begin{pmatrix} \frac{\partial p}{\partial x_1} \\ \frac{\partial p}{\partial x_2} \end{pmatrix}$ is the gradient of pressure in physical domain.

We define the gradient velocity in the parameter space in a similar manner. Due to the compact support that B-splines by design have, only a few basic velocity functions have support above Γ .

Let $n_{int} = n - n_{ext}$ be the number of basis functions with support inside the domain, where n_{ext} be the number of basis functions with marginal support Γ . This is how we organize the functions. Rewriting formula (45) as follows:

$$u_{hk}^j(\xi_1, \xi_2) = \sum_{i=1}^{n_{int}} N_i^{p,q}(\xi_1, \xi_2) u_{ik}^j + \sum_{i=n_{int}+1}^n N_i^{p,q}(\xi_1, \xi_2) u_{ik}^j. \quad (48)$$

The strong aspect is only possible for values of n_{ext} , such as $u_{hk}^j = g_{hk}^j$, by adjusting the speed control variables u_{ik}^j so that the total in the equation process in (48) is close to the value $g^j = (g_{h1}^j, g_{h2}^j)$ in (4). The criteria are fully satisfied if g^j at iteration j is in the function space produced by $N_i^{p,q}$, otherwise, they are only satisfied in the sense of least squares. When it comes to pressure, we can see that equation (1)-(2) simply contains the pressure gradient. We have $m = n_{int}$ because there isn't a pressure control variable that has to be adjusted.

5.2. Matrix form

By dividing the superposition of u into parts with support on the fixed boundary and unbounded parts as in equation (44), reversing the order of summation and integration, and rearrangement, we can approximate the velocity and pressure fields (45)-(46) as an iterative approximation (44) of the governing equations. The problem (44) can then be equivalently transformed into a matrix problem and solved using the required MATLAB code. We have the following matrix system at iteration j :

$$\begin{bmatrix} A_1^{j+1} + N_1^{j+1} & 0 & -B_1^{j+1t} \\ 0 & A_2^{j+1} + N_2^{j+1} & -B_2^{j+1t} \\ B_1^{j+1} & B_2^{j+1} & 0 \end{bmatrix} \begin{bmatrix} w_1^{j+1} \\ w_2^{j+1} \\ p^{j+1} \end{bmatrix} = \begin{bmatrix} f_1^j \\ f_2^j \\ 0 \end{bmatrix} - \begin{bmatrix} A_1^j + N_1^j & 0 \\ 0 & A_2^j + N_2^j \\ B_1^j & B_2^j \end{bmatrix} \begin{bmatrix} w_1^j \\ w_2^j \end{bmatrix}, \quad (49)$$

for all iteration $j = 0, 1, \dots$

$$(A_k^j)_{st} = \int_0^1 \frac{1}{Re} \varepsilon J^{-T} \nabla N_{ks}^{p,q} \cdot J^{-T} \nabla N_{kt}^{p,q} \det(J) d\xi_1 d\xi_2 + \int_0^1 \frac{1}{Re} \alpha N_{ks}^{p,q} N_{kt}^{p,q} (S) \det(J) d\xi_1 d\xi_2, \quad (50)$$



for all iteration $j = 1, 2 \dots$

$$(N_k^j)_{st} = \int_0^1 \beta((w_{1h}^{j-1} + G_{1h}^{j-1})^2 + (w_{2h}^{j-1} + G_{2h}^{j-1})^2)^{\frac{1}{2}} N_{ks}^{p,q}(S) N_{kt}^{p,q}(S) \det(J) d\xi_1 d\xi_1 \tag{51}$$

for all iteration $j = 0, 1 \dots$

$$(B_k^j)_{nm} = \int_0^1 \frac{\partial S}{\partial \xi_k} \frac{\partial N_{kn}^{p,q}}{\partial x_k} N_{km}^{r,s}(S) \det(J) d\xi_1 d\xi_1, \tag{52}$$

for all iteration $j = 0, 1 \dots$

$$(f_k^j)_m = \int_0^1 f_k N_{km}^{p,q}(S) \det(J) d\xi_1 d\xi_1, \tag{53}$$

the integrals presented in equations (50) to (53) are evaluated according to the Gaussian quadrature equation [16].

6. Numerical Discussion

In this section, we perform a numerical validation of the selected elements using three test problems. The first test involves the Navier-Stokes-Brinkman problem, while the second test focuses on the Navier-Stokes problem, conducted within a uniform square domain $[0,1] \times [0,1]$. Subsequently, we employ the chosen elements to solve a two-dimensional Stokes flow problem over a non-standard domain represented by a quarter of an annular region.

In particular, the NURBS-based IGA framework must be emphasized offers an advantage in accurately representing two-dimensional flow within a quarter-annular domain due to its exact geometric representation, a feature not typically found in standard finite element methods. For our numerical simulations in Matlab, we utilize the IGA library GeoPDEs [48]. The error graphs are presented using a log-log scale, where we define the L^2 error and H^1 error as follows:

$$L^2 - norm \quad \|e_h\|_{L^2} = \left(\int_{\Omega} |u_h - u|^2 d\Omega \right)^{\frac{1}{2}}, \tag{54}$$

$$H^1 - norm \quad \|e_h\|_{H^1} = \left(\int_{\Omega} (|u_h - u|^2 + |\nabla u_h - \nabla u|^2) d\Omega \right)^{\frac{1}{2}}, \tag{55}$$

where u represents the exact solution, and u_h is the approximated solution for our problem.

To demonstrate the convergence rate, we employ the following formula:

$$r = \log_2 \left(\frac{|e_{h_{i+1}}|}{|e_{h_i}|} \right), \tag{56}$$

6.1. The Navier-Stokes-Brinkman problem

In this first numerical validation test, we focus on the Navier-Stokes-Brinkman problem on the square domain $[0,1] \times [0,1]$; in porous media, Darcy's equation must be considered, Soullaine et al. [54] have analyzed the effect on permeability of sub-resolution porosity in X-ray micro-CT images. When micro-porosity at the pore scale is taken into account, the Navier-Stokes equations are not adequate to solve the flow. This brings us back to the Navier-Stokes-Brinkman equations, the system is written in the form:

$$-div(\nu \nabla u - u \otimes u) + \frac{1}{\varrho} \nabla p + \frac{\alpha}{Re} u = f \text{ in } \Omega, \tag{57}$$

$$-div u = 0 \text{ in } \Omega, \tag{58}$$

subject to the boundary conditions, the Dirichlet boundary $u = 0$ on $\{x = 0 \text{ and } 0 \leq y \leq 1\} \cup \{x = 1 \text{ and } 0 \leq y \leq 1\}$ and the Neuman boundary otherwise, the coefficients $\varrho = \nu = 1$ and $Re = \alpha = 20$.

Figures 3 and 4 show the solution to the velocity and pressure of the problem (57) and (58) with mesh elements 32×32 .

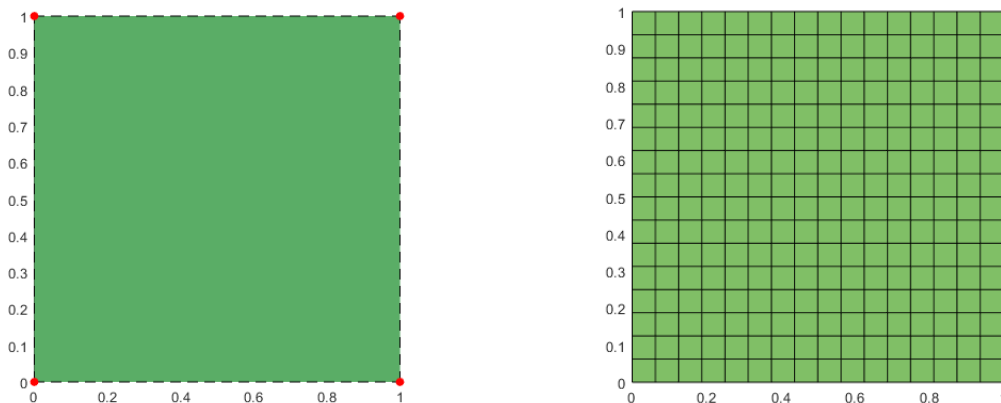


Fig. 2. Plot a NURBS entity along with its control points (left) and 16×16 elements mesh (right).



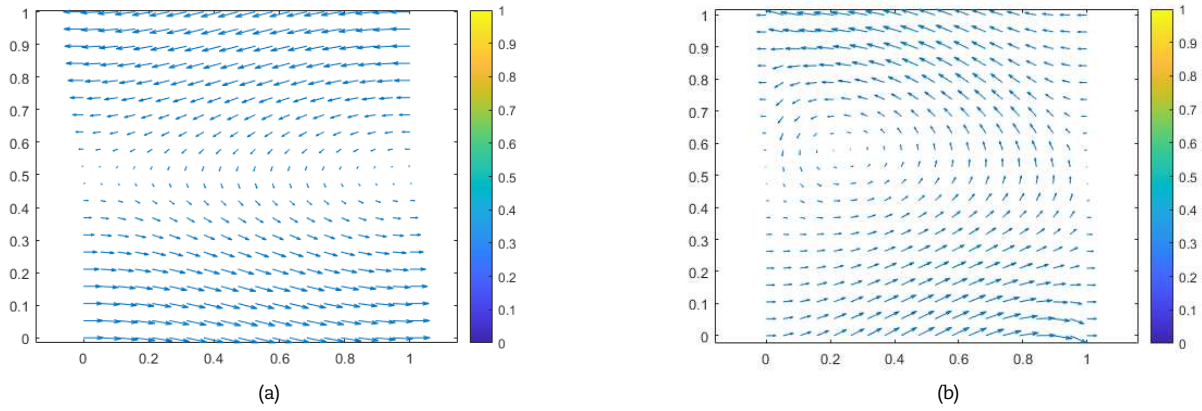


Fig. 3. Computed velocity for (a) $\nu = 1$ and (b) $\nu = 0.1$.

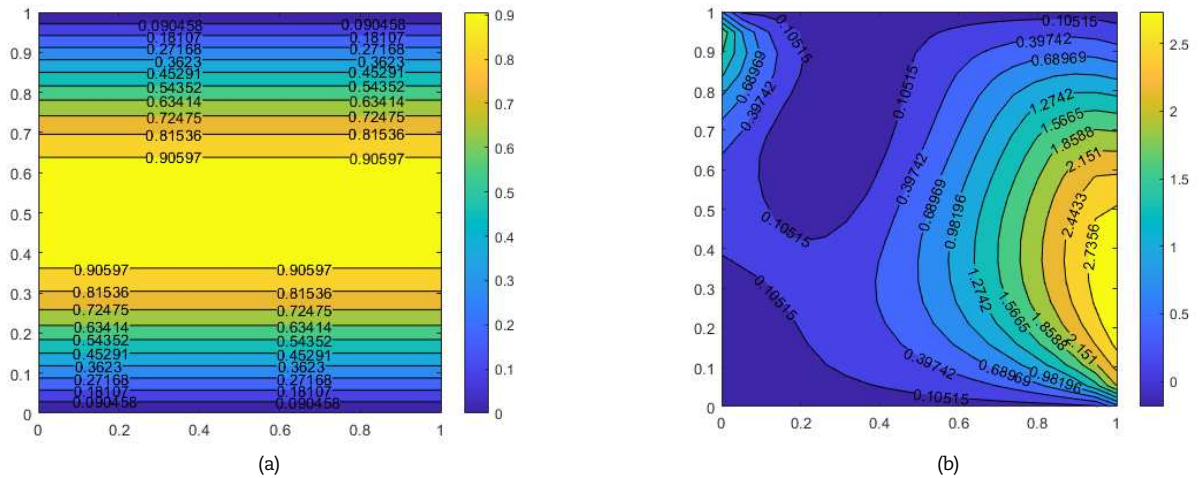


Fig. 4. Computed pressure for (a) $\nu = 1$ and (b) $\nu = 0.1$.

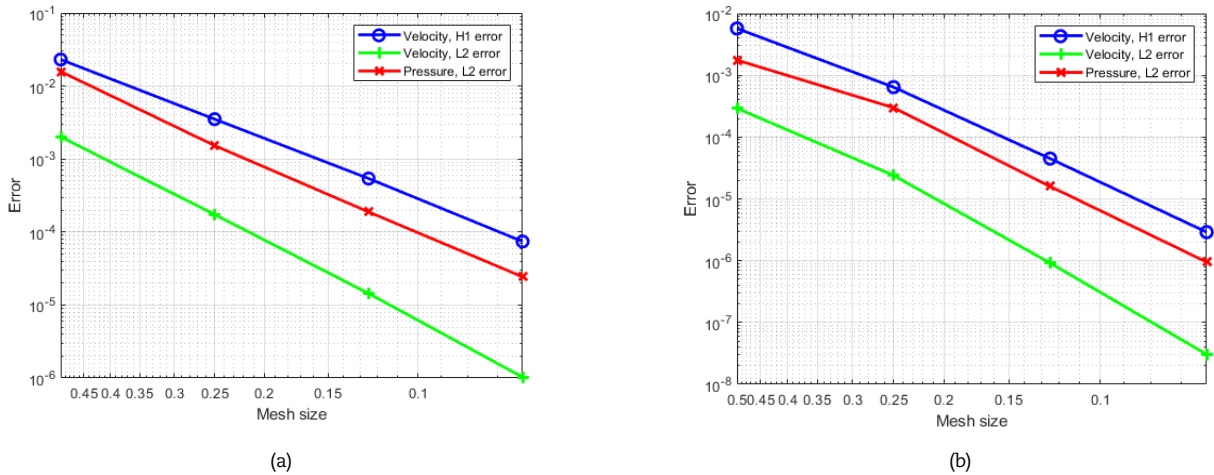


Fig. 5. The convergence error of the IGA method for example (59), for (a) $p = 2$ and (b) $p = 3$.

In the first example, two tests are presented by changing the ν value between two values $\nu = 1$ and $\nu = 0.1$, the two diagrams in Fig. 3 show the flow velocity we notice that the velocity makes a rotation in the center of the cube and this rotation makes a displacement towards the left in the case of the value $\nu = 0.1$, in Fig. 4 we have shown the plot of the pressure, the two diagrams give two quite different results concerning the values of the pressure knowing that the maximum appears in the channel center but in the case of the value $\nu = 0.1$ the maximum pressure is concentrated in the right wall.

On the other hand, Figs. 5 and 6 show the convergence of the method described in this document, of which the exact solution of the problem (57) and (58) is:

$$u(x, y) = \begin{pmatrix} \cos(\pi y) \\ x(x - 1) \end{pmatrix}, \quad p(x, y) = \sin(\pi y). \tag{59}$$

on elements 8×8 , 16×16 , 32×32 and 64×64 , successively. We calculated convergence for discretization of NURBS method with different mesh sizes and polynomial degrees for the solution presented above.



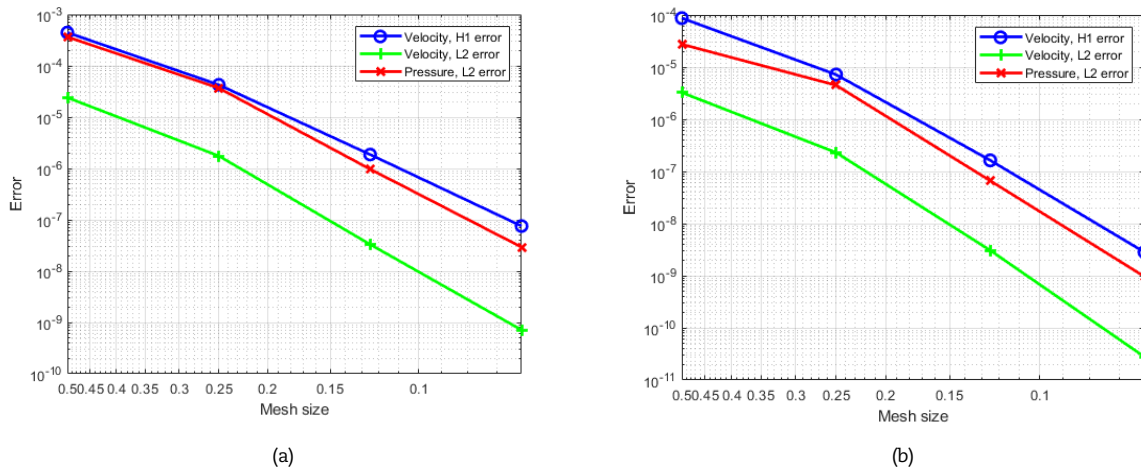


Fig. 6. The convergence error of the IGA method for example (59), for (a) $p = 4$ and (b) $p = 5$.

These graphs show the error between the approximate solution obtained using the NURBS method and the analytical solution, which tends towards zero from step $h = 0.35$, so we can stop the refinement process at this step. The improvement in the convergence of this method also depends on the degree of the NURBS basis functions in fact; if the degree is higher, the convergence should be enhanced.

6.2. The Navier-Stokes problem

In this second numerical validation test, we focus on the Navier-Stokes problem on the square domain $[0,1] \times [0,1]$, so the system become in the form:

$$-div(\nu \nabla u - u \otimes u) + \frac{1}{\rho} \nabla p = f \text{ in } \Omega, \tag{60}$$

$$div u = 0 \text{ in } \Omega, \tag{61}$$

Other applicative results can be found in [48-53]. On the next part, we present the convergence of the method described in this document and an error comparison between IGA method and virtual finite element method presented in [55] of which the exact solution of the problem (60)-(61) presented below:

$$u(x, y) = \frac{1}{2} \begin{pmatrix} \sin(2\pi x)^2 \sin(2\pi y) \cos(2\pi y) \\ -\sin(2\pi y)^2 \sin(2\pi x) \cos(2\pi x) \end{pmatrix}, \quad p(x, y) = \pi^2 \sin(2\pi x) \cos(2\pi y), \tag{62}$$

subject to the boundary conditions mixes, the Dirichlet boundary $u = 0$ on Γ , the polynomial degree of pressure of accuracy for the numerical tests is $p = 2$. The coefficients $\rho = 1$ and ν equal to the values described in the presented Tables below.

We calculated convergence rates for discretization of divergence-conforming B-splines with different mesh sizes and polynomial degrees for the solution presented above. Additionally, we have calculated the convergence rates, which show in the Tables 1 and 2 the superiority of the IGA method over the virtual element method.

Tables 3 and 4 show the error between the approximate solution obtained by the NURBS method and the analytical solution of the velocity and the pressure in the case of the value of $\nu = 0.1$, these errors tend towards zero from the step of mesh size element 16×16 , so that we can stop the refinement process at this step. The improvement in the convergence of this method also depends on the degree of the NURBS basis functions. Indeed, as long as the degree is high, convergence should be improved.

Table 1. Computational results for error velocity, $\nu = 1$.

h	$\ u - u_h\ _{H^1}$ for IGA	Rate	$\ u - u_h\ _{H^1}$ for VEM presented in [55]	Rate
8×8	6.66963393421790 e-03	-	3.704032467 e-01	-
16×16	5.81279613701919 e-04	2.44	9.153568669 e-02	1.3979
32×32	4.25351230864542 e-05	2.61	2.308710367 e-02	1.3775
64×64	2.82176996432552 e-06	2.71	5.791512013 e-03	1.3829

Table 2. Computational results for the error pressure, $\nu = 1$.

h	$\ p - p_h\ _{L^2}$ for IGA	Rate	$\ p - p_h\ _{L^2}$ for VEM presented in [55]	Rate
8×8	2.8 e-03	-	3.891840615 e-01	-
16×16	2.0 e-04	2.63	8.875084726 e-02	1.47
32×32	1.0 e-05	2.99	1.994452869 e-02	1.49
64×64	1.0 e-06	2.30	4.602515029 e-03	1.46



Table 3. Computational results for the error velocity, $\nu = 0.1$.

h	$\ u - u_h\ _{L^2}$ for IGA	Rate	$\ u - u_h\ _{H^1}$ for IGA	Rate
8×8	5.07031249748252 e-04	-	2.32102058964810 e-02	-
16×16	1.00975415854364 e-05	3.91	9.91435454703094 e-04	3.15
32×32	2.63950472295762 e-07	3.64	5.14779797398132 e-05	2.95
64×64	7.89815968581328 e-09	3.50	3.02116817673976 e-06	2.83

Table 4. Computational results for the error pressure, $\nu = 0.1$.

h	$\ p - p_h\ _{L^2}$ for IGA with $p = 3$	Rate	$\ p - p_h\ _{L^2}$ for IGA with $p = 4$	Rate
8×8	2.84312853887740 e-03	-	0.00367109854741338	-
16×16	1.53437182020196 e-04	2.91	9.34388062481364e-05	3.67
32×32	9.24222816025140 e-06	2.80	2.93519480732800e-06	3.46
64×64	5.73931700590064 e-07	2.77	9.31368949289397e-08	3.45

6.3. The Stokes problem

We will now present a few examples to demonstrate the convergence order of the IGA approximation towards the continuous solution on a no standard domain. It is important to note that the Stokes problem as a special case to problem (1) and (2). Therefore, we focus on the Stokes problem within one quarter of an annulus domain $[1,2] \times [0, \frac{\pi}{3}]$. The system is expressed in the following form:

$$-div(\nu \nabla u) + \frac{1}{\rho} \nabla p = f \text{ in } \Omega, \tag{63}$$

$$-div u = 0 \text{ in } \Omega, \tag{64}$$

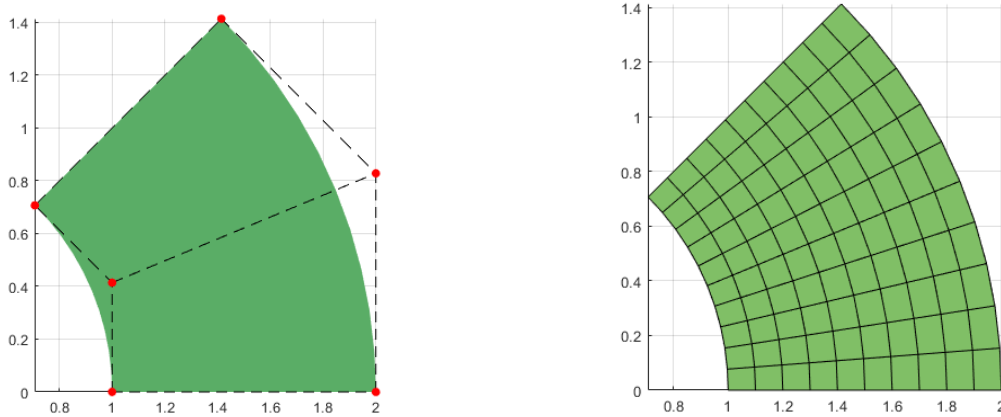


Fig. 7. Plot a NURBS entity along with its control points (left) and 10×10 elements mesh (right).

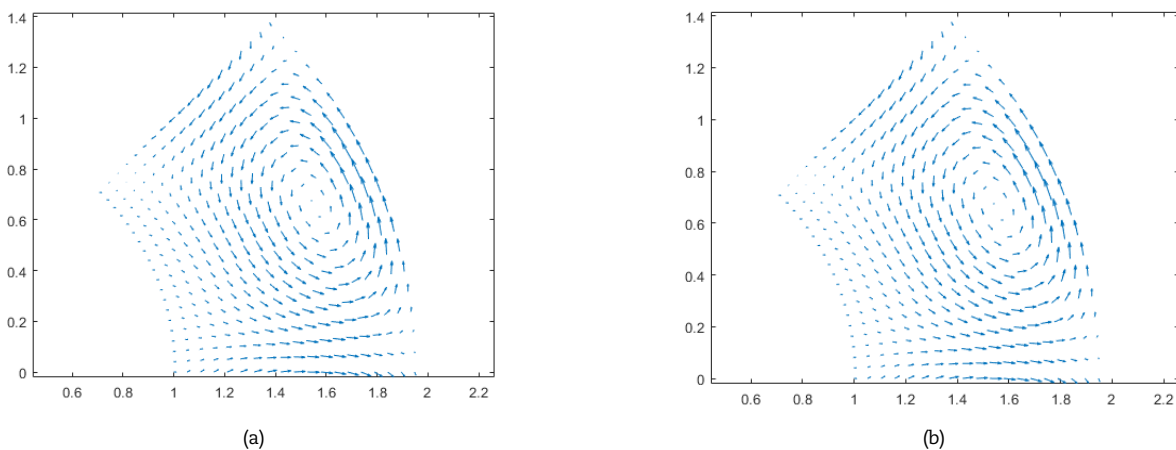


Fig. 8. Computed velocity for 10×10 elements, (a) $p = 3$ and (b) $p = 4$.



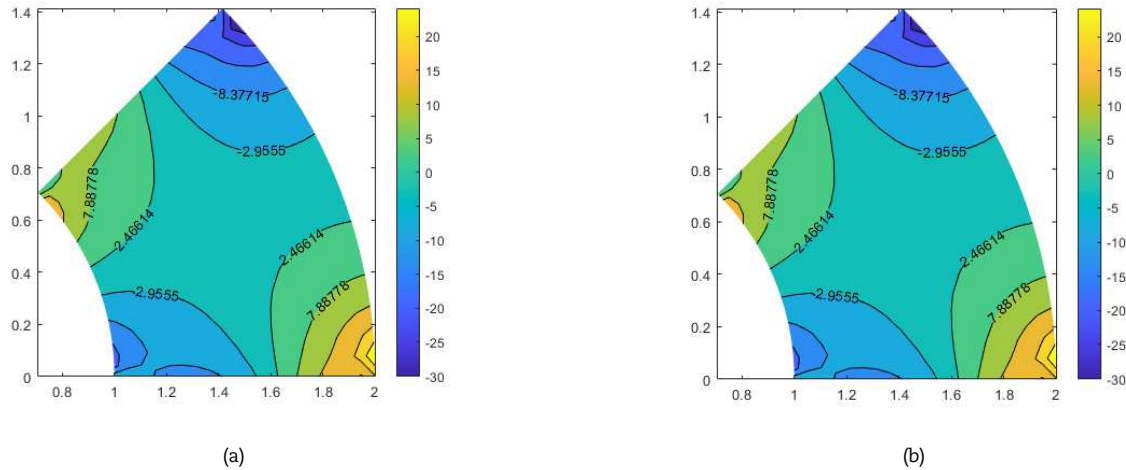


Fig. 9. Computed pressure for 10×10 elements, (a) $p = 3$ and (b) $p = 4$.

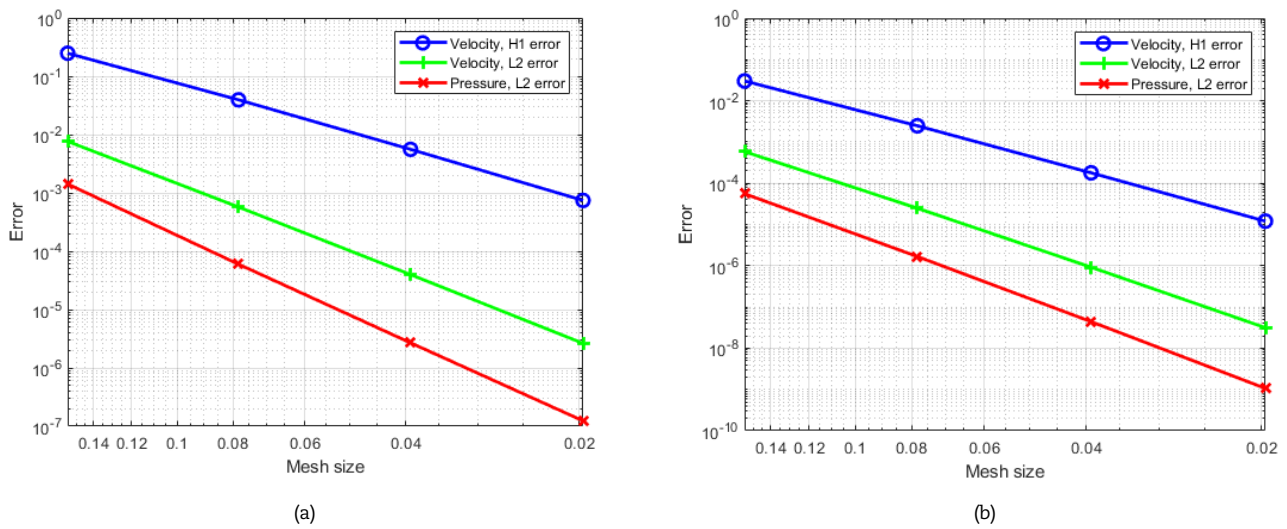


Fig. 10. The convergence error of the IGA method for example (65) for (a) $p = 2$ and (b) $p = 3$.

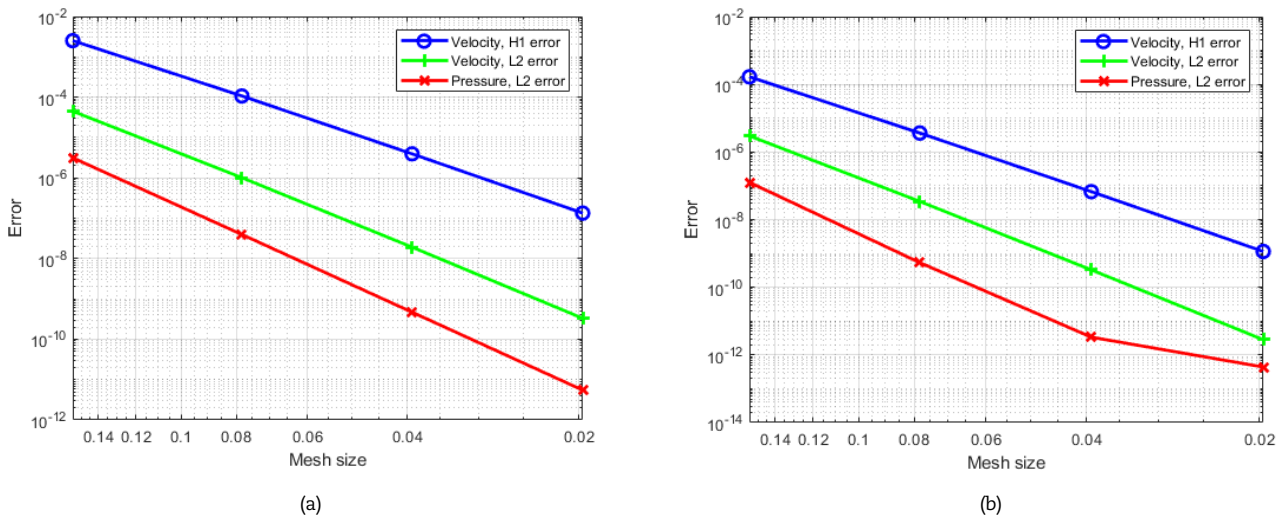


Fig. 11. The convergence error of the IGA method for example (65) for (a) $p = 4$ and (b) $p = 5$.

subject to the Dirichlet boundary $u = g$, for this test g takes the values of exact solution on $\partial\Omega$, the coefficients $\rho = 1$ and ν equal to 1. Figures 8 and 9 show the solution to the velocity and pressure problem with mesh elements 10×10 for pressure space degree $p = 3$ and $p = 4$.

On the other hand, Figs. 10 and 11 show the convergence of the method described in this document, of which the exact solution of the problem (63)-(64) is:



$$\begin{aligned}
u_1(x, y) &= (2(x-y)y(-4+x^2+y^2)(-1+x^2+y^2)(x^5-8y-2x^4y+20y^3-6y^5+ \\
&\quad 2x^2y(5-4y^2)+x^3(-5+6y^2)+x(4+5y^2(-3+y^2))), \\
u_2(x, y) &= (-2(x-y)y^2(-4+x^2+y^2)(-1+x^2+y^2)(4+5x^2(-3+ \\
&\quad x^2)+2x(5-2x^2)y+(-5+6x^2)y^2-4xy^3+y^4)), \\
p(x, y) &= -\left(\frac{\pi}{8}\right) + \operatorname{atan}\frac{y}{x}.
\end{aligned} \tag{65}$$

on elements 8×8 , 16×16 , 32×32 and 64×64 , successively.

These graphs show the error between the approximate solution obtained using the NURBS method and the analytical solution for Stokes problem, which tends towards zero from step $h = 0.12$, so we can stop the refinement process at this step. The improvement in the convergence of this method also depends on the degree of the NURBS basis functions in fact; as long as the degree is higher, the convergence should be enhanced.

7. Conclusion

We have established the well-posedness of the DBF model with Dirichlet boundary conditions in its variational form, with a focus on the flow aspect. To represent the solution, we utilized NURBS functions within the functional space. Additionally, we formulated the algebraic problem and computed the elements of the resulting matrices. For approximating integrals, we employed the Gauss quadrature method.

In the numerical section of the paper, we have presented three examples to demonstrate the error estimates and the effectiveness of the proposed numerical method, from this numerical study, we concluded that:

- The convergence of the error by comparing it with an analytical solution. As the mesh is refined, the error approaches nearly zero.
- The convergence of the error by comparing it with an analytical solution. As the degree of NURBS basis functions is raised.
- We can see that in order to guarantee more rapid convergence, it is sufficient to choose a NURBS basis functions with a high degree.
- The NURBS method guarantees an exact representation of the geometry as presented in the quarter ring in Fig. 7 which makes it possible to eliminate the error resulting from the geometric representation by comparing with the classic finite elements whose these type of errors exist.
- The convergence rate of the NURBS method is higher than that of the virtual elements method, in fact as shown in Table 1, for the mesh size 16×16 the rate of IGA is 2.44 and 1.3979 for VEM.

Author Contributions

All authors contributed to the conceptualization and methodology of the study. O. Koubaiti provided the mathematical theoretical background, L. El Ouadefli performed the tests simulation, A. Elkhalfi, A. El Akkad, S. Vlase and M. Marin supervised the work and reviewed and edited the manuscript. All authors discussed the results, reviewed and approved the final version of the manuscript.

Acknowledgments

No applicable.

Conflict of Interest

The authors declared no potential conflicts of interest concerning the research, authorship, and publication of this article.

Funding

The authors received no financial support for the research, authorship, and publication of this article.

Data Availability Statements

No applicable.

Nomenclature

R_e	Reynolds number	B_i^d	B-spline basis
U_i	Mean velocity components ($i = 1, 2, 3$)	ε	Porosity
$N_{i,j}^{p,q}$	NURBS basis	J	Jacobian matrix
p	Pressure	ρ	Constant density
u	Velocity	ν	Constant kinematic viscosity
σ	Frictional force		

References

- [1] Vafai, K., Convective flow and heat transfer in variable-porosity media, *Journal of Fluid Mechanics*, 147, 1984, 233-259.
[2] Varsakelis, C., Papalexandris, M.V., On the well-posedness of the Darcy–Brinkman–Forchheimer equations for coupled porous media-clear fluid flow, *Nonlinearity*, 30(4), 2017, 1449.




- [3] Whitaker, S., *The method of volume averaging*, Springer Science & Business Media, 13, 1998.
- [4] Whitaker, S., The Forchheimer equation: a theoretical development, *Transport in Porous Media*, 25(1), 1996, 27-61.
- [5] Tayebi, T., Chamkha, A.J., Öztop, H.F., Bouzeroura, L., Local thermal non-equilibrium (LTNE) effects on thermal-free convection in a nanofluid-saturated horizontal elliptical non-Darcian porous annulus, *Mathematics and Computers in Simulation*, 194, 2022, 124-140.
- [6] Tayebi, T., Analysis of the local non-equilibria on the heat transfer and entropy generation during thermal natural convection in a non-Darcy porous medium, *International Communications in Heat and Mass Transfer*, 135, 2022, 106133.
- [7] Tayebi, T., Chamkha, A.J., Analysis of the effects of local thermal non-equilibrium (LTNE) on thermo-natural convection in an elliptical annular space separated by a nanofluid-saturated porous sleeve, *International Communications in Heat and Mass Transfer*, 129, 2021, 105725.
- [8] Kaloni, P.N., Guo, J., Steady nonlinear double-diffusive convection in a porous medium based upon the Brinkman-Forchheimer model, *Journal of Mathematical Analysis and Applications*, 204(1), 1996, 138-155.
- [9] Fabes, E., Kenig, C., Verchota, G., The Dirichlet problem for the Stokes system on Lipschitz domains, *Duke Mathematical Journal*, 57, 1988, 769-793.
- [10] Choe, H., Kim, H., Dirichlet problem for the stationary Navier-Stokes system on Lipschitz domains, *Communications in Partial Differential Equations*, 36, 2011, 1919-1944.
- [11] Scutaru, M.L., Guendaoui, S., Koubaiti, O., El Ouadefli, L., El Akkad, A., Elkhalfi, A., Vlase, S., Flow of Newtonian Incompressible Fluids in Square Media: Isogeometric vs. Standard Finite Element Method, *Mathematics*, 11(17), 2023, 3702.
- [12] Discacciati, M., Quarteroni, A., Navier-Stokes/Darcy coupling: modeling, analysis, and numerical approximation, *Revista Matemática Complutense*, 22(2), 2009, 315-426.
- [13] Galdi, G., *An introduction to the mathematical theory of the Navier-Stokes equations: Steady-state problems*, Springer Science Business Media, 2011.
- [14] Girault, V., Riviere, B.D.G., Approximation of coupled Navier-Stokes and Darcy equations by Beaver-Joseph-Saffman interface condition, *SIAM Journal on Numerical Analysis*, 47(3), 2009, 2052-2089.
- [15] Temam, R., *Navier-Stokes equations: theory and numerical analysis*, Vol. 343, American Mathematical Soc., 2001.
- [16] Hughes, T.J., Reali, A., Sangalli, G., Efficient quadrature for NURBS-based isogeometric analysis, *Computer Methods in Applied Mechanics and Engineering*, 199(5-8), 2010, 301-313.
- [17] El Ouadefli, L., El Akkad, A., El Moutea, O., Moustabchir, H., Elkhalfi, A., Luminita Scutaru, M., Muntean, R., Numerical simulation for Brinkman system with varied permeability tensor, *Mathematics*, 10(18), 2022, 3242.
- [18] El Ouadefli, L., Moutea, O.E., Akkad, A.E., Elkhalfi, A., Vlase, S., Scutaru, M.L., Mixed Isogeometric Analysis of the Brinkman Equation, *Mathematics*, 11(12), 2023, 2750.
- [19] Koubaiti, O., EL Fakkoussi, S., El-Mekkaoui, J., Moustachir, H., Elkhalfi, A., Pruncu, C.I., The treatment of constraints due to standard boundary conditions in the context of the mixed Web-spline finite element method, *Engineering Computations*, 38(7), 2021, 2937-2968.
- [20] Koubaiti, O., El-mekkaoui, J., Elkhalfi, A., Complete study for solving Navier-Lamé equation with new boundary condition using mini element method, *International Journal of Mechanics*, 12, 2018, 46-58.
- [21] EL Fakkoussi, S., Vlase, S., Marin, M., Koubaiti, O., Elkhalfi, A., Moustabchir, H., Predicting Stress Intensity Factor for Aluminum 6062 T6 Material in L-Shaped Lower Control Arm (LCA) Design Using Extended Finite Element Analysis, *Materials*, 17, 2024, 206.
- [22] Montassir, S., Moustabchir, H., Elkhalfi, A., Scutaru, M.L., Vlase, S., Fracture modelling of a cracked pressurized cylindrical structure by using extended iso-geometric analysis (x-iga), *Mathematics*, 9(23), 2021, 2990.
- [23] El-Mekkaoui, J., Elkhalfi, A., Elakkad, A., Resolution of Stokes Equations with the Ca,b Boundary Condition Using Mixed Finite Element Method, *WSEAS Transactions on Mathematics*, 12, 2013, 586-597.
- [24] Hughes, T.J., Cottrell, J.A., Bazilevs, Y., Isogeometric analysis: CAD, finite elements, NURBS, exact geometry and mesh refinement, *Computer Methods in Applied Mechanics and Engineering*, 194(39-41), 2005, 4135-4195.
- [25] Cottrell, J.A., Hughes, T.J., Bazilevs, Y., *Isogeometric analysis: toward integration of CAD and FEA*, John Wiley & Sons, 2009.
- [26] Gomez, H., Hughes, T.J., Nogueira, X., Calo, V.M., Isogeometric analysis of the isothermal Navier-Stokes-Korteweg equations, *Computer Methods in Applied Mechanics and Engineering*, 199(25-28), 2010, 1828-1840.
- [27] Beirão da Veiga, L., Buffa, A., Rivas, J., Sangalli, G., Some estimates for h-p-k-refinement in isogeometric analysis, *Numerische Mathematik*, 118, 2011, 271-305.
- [28] Benson, D.J., Bazilevs, Y., Hsu, M.C., Hughes, T., A large deformation, rotation-free, isogeometric shell, *Computer Methods in Applied Mechanics and Engineering*, 200(13-16), 2011, 1367-1378.
- [29] Auricchio, F., da Veiga, L.B., Buffa, A., Lovadina, C., Reali, A., Sangalli, G., A fully "locking-free" isogeometric approach for plane linear elasticity problems: A stream function formulation, *Computer Methods in Applied Mechanics and Engineering*, 197(1-4), 2007, 160-172.
- [30] Ergun, S., Fluid flow through packed columns, *Chemical Engineering Progress*, 48(2), 1952, 89-94.
- [31] Seidel-Morgenstern, A. (Ed.), *Membrane reactors: distributing reactants to improve selectivity and yield*, John Wiley & Sons, 2010.
- [32] Bey, O., *Strömungsverteilung und Wärmetransport in Schüttungen*, VDI-Verlag, 1998.
- [33] Vafai, K., Kim, S., On the limitations of the Brinkman-Forchheimer-extended Darcy equation, *International Journal of Heat and Fluid Flow*, 16(1), 1995, 11-15.
- [34] Hornung, U. (Ed.), *Homogenization and porous media*, Vol. 6, Springer Science & Business Media, 2012.
- [35] Garibotti, C.R., Peszynska, M., Upscaling non-Darcy flow, *Transport in Porous Media*, 80, 2009, 401-430.
- [36] Matossian, V., Bhat, V., Parashar, M., Peszynska, M., Sen, M., Stoffa, P., Wheeler, M.F., Autonomic oil reservoir optimization on the grid, *Concurrency and Computation: Practice and Experience*, 17(1), 2005, 1-26.
- [37] Winterberg, M., Tsotsas, E., Modelling of heat transport in beds packed with spherical particles for various bed geometries and/or thermal boundary conditions, *International Journal of Thermal Sciences*, 39(5), 2000, 556-570.
- [38] Nield, D.A., Bejan, A., *Convection in porous media*, Springer, New York, 2006.
- [39] Skrzypacz, P., Wei, D., Solvability of the Brinkman-Forchheimer-darcy equation, *Journal of Applied Mathematics*, 2017, 2017, 7305230.
- [40] Hughes, T.J., Cottrell, J.A., Bazilevs, Y., Isogeometric analysis: CAD, finite elements, NURBS, exact geometry and mesh refinement, *Computer Methods in Applied Mechanics and Engineering*, 194(39-41), 2005, 4135-4195.
- [41] Cocquet, P.H., Rakotobe, M., Ramalingom, D., Bastide, A., Error analysis for the finite element approximation of the Darcy-Brinkman-Forchheimer model for porous media with mixed boundary conditions, *Journal of Computational and Applied Mathematics*, 381, 2021, 113008.
- [42] Sayah, T., A posteriori error estimates for the Brinkman-Darcy-Forchheimer problem, *Computational and Applied Mathematics*, 40, 2021, 1-38.
- [43] Hughes, T.J., Reali, A., Sangalli, G., Efficient quadrature for NURBS-based isogeometric analysis, *Computer Methods in Applied Mechanics and Engineering*, 199(5-8), 2010, 301-313.
- [44] Girault, V., Raviart, P.A., *Finite element approximation of the Navier-Stokes equations*, Vol. 749, Springer, Berlin, 1979.
- [45] Girault, V., Raviart, P.A., *Finite element methods for Navier-Stokes equations: theory and algorithms*, (Vol. 5, Springer Science & Business Media, 2012.
- [46] Tagliabue, A., Dede, L., Quarteroni, A., Isogeometric analysis and error estimates for high order partial differential equations in fluid dynamics, *Computers & Fluids*, 102, 2014, 277-303.
- [47] Cayco, M.E., Nicolaidis, R.A., Finite element technique for optimal pressure recovery from stream function formulation of viscous flows, *Mathematics of Computation*, 46(174), 1986, 371-377.
- [48] Vázquez, R., A new design for the implementation of isogeometric analysis in Octave and Matlab: GeOPDEs 3.0, *Computers & Mathematics with Applications*, 72(3), 2016, 523-554.
- [49] Vlase, S., Dynamical response of a multibody system with flexible elements with a general three-dimensional motion, *Romanian Journal of Physics*, 57(3-4), 2012, 676-693.
- [50] Vlase, S., Danasel, C., Scutaru, M.L., Mihalcica, M., Finite element analysis of a two-dimensional linear elastic systems with a plane "rigid motion", *Romanian Journal of Physics*, 59(5-6), 2014, 476-487.
- [51] Marin, M., Seadawy, A., Vlase, S., Chirila, A., On mixed problem in thermoelasticity of type III for Cosserat media, *Journal of Taibah University for Science*, 16(1), 2022, 1264-1274.
- [52] Othman, M.I., Fekry, M., Marin, M., Plane waves in generalized magneto-thermo-viscoelastic medium with voids under the effect of initial stress and laser pulse heating, *Structural Engineering and Mechanics*, 73(6), 2020, 621-629.




- [53] Abbas, I., Hobiny, A., Marin, M., Photo-thermal interactions in a semi-conductor material with cylindrical cavities and variable thermal conductivity, *Journal of Taibah University for Science*, 14(1), 2020, 1369-1376.
- [54] Soulaine, C., Gjetvaj, F., Garing, C., Roman, S., Russian, A., Gouze, P., Tchelepi, H.A., The impact of sub-resolution porosity of X-ray microtomography images on the permeability, *Transport in Porous Media*, 113, 2016, 227-243.
- [55] Beirão da Veiga, L., Mora, D., Vacca, G., The Stokes complex for virtual elements with application to Navier–Stokes flows, *Journal of Scientific Computing*, 81, 2019, 990-1018.


ORCID iD


Ouadie Koubaiti  <https://orcid.org/0000-0002-0045-3128>

Lahcen El Ouadefli  <https://orcid.org/0009-0005-0572-0116>

Ahmed Elkhalfi  <https://orcid.org/0000-0001-9861-8316>

Abdeslam El Akkad  <https://orcid.org/0000-0002-5907-9599>

Sorin Vlase  <https://orcid.org/0000-0001-8679-2579>

Marin Marin  <https://orcid.org/0000-0003-1552-3763>



© 2024 Shahid Chamran University of Ahvaz, Ahvaz, Iran. This article is an open access article distributed under the terms and conditions of the Creative Commons Attribution-NonCommercial 4.0 International (CC BY-NC 4.0 license) (<http://creativecommons.org/licenses/by-nc/4.0/>).

How to cite this article: Koubaiti O., El Ouadefli L., Elkhalfi A., El Akkad A., Vlase S., Marin M. Isogeometric Resolution of the Brinkman-Forchheimer-Darcy, *J. Appl. Comput. Mech.*, xx(x), 2024, 1–14. <https://doi.org/10.22055/jacm.2024.45440.4366>

Publisher's Note Shahid Chamran University of Ahvaz remains neutral with regard to jurisdictional claims in published maps and institutional affiliations.

